Tidal modulation of seabed light and its implications for benthic algae

Roberts, Emyr; Bowers, David; Davies, Andrew

Limnology and Oceanography

DOI:
10.1002/lno.10616

Published: 01/01/2018

Peer reviewed version

Tidal modulation of seabed light and its implications for benthic algae

Emyr Martyn Roberts[1], David George Bowers[1], and Andrew John Davies[1]

[1]*School of Ocean Sciences, Bangor University, Menai Bridge, Anglesey, UK LL59 5AB*

Corresponding author's email address (E.M. Roberts): emyr.roberts@bangor.ac.uk

Running head: Tidal modulation of seabed light

Keywords: light, tides, algae, growth, photosynthesis

Abstract

The temporal behaviour of seabed light in a shallow, tidal sea is set largely by the interaction of the solar elevation cycle with tidal cycles in water depth and temporal variability in water clarity. The effect of tidal modulation on seabed light often does not simply average out, producing instead a net effect (either an amplification or a reduction of seabed light, integrated over time) compared to a tideless, but otherwise equivalent, scenario. Observations of this phenomenon from the Bay of Brest (France) show reasonable agreement with predictions based on an earlier theoretical framework, confirming that the key physics has been understood and that the important parameters are tidal amplitude, timing of low waters, diffuse attenuation coefficient, and daylength. Implications for benthic macroalgae living in the bay's shallow subtidal zone are investigated using a simple numerical model. The effects of the tide on time-integrated seabed light and, in turn, time-integrated macroalgal community photosynthesis in the Bay of Brest correspond closely at three timescales: annual, springs-neaps (i.e., approximately fortnightly), and daily. Tidal amplification of both parameters occurs over the year, during winter months generally, and at spring tides during winter specifically (slight reduction occurs at neaps during winter). For an individual, isolated thallus, the relationship between tidal modulation of seabed light and photosynthesis is complicated by more pronounced light-saturation and photoinhibition effects. Demonstrated here for the first time, neglecting tidal effects on seabed light is likely to result in

erroneous estimates (and, for many sites, underestimation) of subtidal benthic productivity.

Introduction

Shallow-water benthic ecosystems, such as kelp forests and seagrass meadows, can be highly productive (Mann, 1972). They also serve as nurseries, habitats, and refugia for many species of marine fauna (Steneck et al., 2002; Heck et al., 2003). Light availability is often the most important abiotic factor regulating the growth patterns, distribution, and primary productivity of benthic algae and plants (Zimmerman et al., 1994, and references therein). As noted by Ackleson (2003), we must continue to refine our understanding of the influence of seabed light on these ecosystems if we are to better predict their response to short-term changes (e.g., storms and pollution events) and long-term changes (e.g., climate and sea-level), and if we are to better quantify their role within the global ocean carbon cycle.

In a tideless (or 'non-tidal') sea, irradiance at the seabed is controlled largely by the daily and seasonal cycles of solar elevation, which govern sea surface irradiation, and by the water depth and clarity, which together determine the extent to which incident light is attenuated before it reaches the bed (Bowers and Brubaker, 2010). In a 'tidal' sea, cycles in water depth (and any associated cycles in water clarity) produce more complicated temporal patterns in seabed irradiance (e.g., Topliss et al., 1980; Pilgrim and Millward, 1989; Bowers et al., 1997; Bowers and Brubaker, 2004). Whilst these patterns may influence the behaviour of benthic animals (Naylor, 2010) and the time course of benthic photosynthesis (Gévaert et

al., 2002, 2003), the principal value of such tidal modulation lies in its potential to result in a net effect on seabed irradiance (and photosynthesis) integrated over time (Bowers and Brubaker, 2010).

Bowers and Brubaker (2010) hypothesised that the tide will tend to amplify the daily total seabed irradiance compared to a scenario with no tide, but with the same mean depth and clarity. They reasoned that light is attenuated in an approximately exponential manner with increasing water depth, and so the 'gains' in irradiance around low-waters should exceed the 'losses' around high-waters (see Fig. 1), leading to a net gain, or amplification, over time (relative to the 'non-tidal' scenario). They went on to demonstrate that the effect is more complicated than the initial premise. The tide can also reduce the daily total seabed irradiance, and the magnitude of the effect depends upon four key parameters: the time of low water, the tidal amplitude (or range), the diffuse attenuation coefficient (a measure of the turbidity of the water), and the daylength.

The ecological implications of the study by Bowers and Brubaker (2010) were potentially very significant, and warrant further investigation. In particular, models that ignore the tide (and use instead a mean water depth) were claimed to underestimate seabed irradiance and may, therefore, also underestimate benthic primary production. Given that the relationship between irradiance and photosynthesis is non-linear (see 'Theory' below and standard texts such as Hurd et al. (2014)), it is unclear whether a large tidal amplification of seabed light will cause a similar amplification of photosynthesis in benthic algae: gains in irradiance at low water will not

necessarily result in equivalent gains in photosynthesis if saturation or photoinhibition occur.

The purpose of the present paper is twofold: (1) to test the original theory against irradiance observations from a new site, the Bay of Brest in France (n.b., the theory has thus far been validated using data from one site only, the Menai Strait in Wales, UK), and (2) to further investigate the ecological implications of Bowers and Brubaker (2010) by the construction of a simple numerical model.

The Bay of Brest was selected on the basis that it is a macrotidal site with tidal and turbidity characteristics that differ from those of the Menai Strait. The Bay of Brest is less turbid, and low waters of spring tides (LWST) always occur at about midday and midnight (i.e., opposite to the case at the Menai Strait, where high waters of spring tides (HWST) occur at these times). Large tidal ranges at spring tides and the coincidence of LWST with the midday peak in sea surface irradiance create a potential for large tidal irradiance amplification. A novel mooring design was employed to measure, rather than infer (as in the original study), 'non-tidal' irradiance. The numerical model has been used to investigate the likely effect of the tide on seabed irradiance and benthic photosynthesis in the Bay of Brest over three timescales (i.e., daily, springs-neaps cycle, and annual) and for two ecological entities (i.e., the individual, isolated kelp thallus, and the established macroalgal community).

Theory

Tidal irradiance amplification

Irradiance at the seabed, I_B, is given by the Lambert-Beer Law,

$$I_B(t) = I_0(t) \exp\left[-k_{PAR}(t) z(t)\right], \tag{1}$$

where I_0 is the sea surface irradiance, k_{PAR} is the diffuse attenuation coefficient of photosynthetically active radiation (PAR), z is the water depth, and t is time. The law typically applies to monochromatic light, but it also applies approximately to irradiance integrated over the PAR waveband (i.e., approximately 400-700 nm) (Kirk, 1994), as required here. Daily total seabed irradiance is determined by integrating the expression above over time.

Bowers and Brubaker (2010) defined a daily tidal irradiance amplification factor, F, as the ratio of the daily total seabed irradiance in a 'tidal' scenario to that in an equivalent 'non-tidal' scenario. Initially, they represented tidal variation in water depth as $z_T = z_0 - b\cos\left(\omega(t - t_{lw})\right)$, where z_0 is the mean water depth, b is the tidal amplitude, ω is the angular frequency of the tide (approximately 0.5 rad h^{-1} for a semi-diurnal tide), t is time and t_{lw} is the time of low water (both measured relative to midday). Water depth in the equivalent non-tidal scenario, z_{NT}, was taken to be z_0. F was therefore given as

$$F = \frac{< I_{BT} >}{< I_{BNT} >} \tag{2}$$

$$= \frac{\int_{-L/2}^{L/2} I_0(t) \exp\left[-k_{PAR}(t)(z_0 - b\cos(\omega(t - t_{lw})))\right] \, \mathrm{d}t}{\int_{-L/2}^{L/2} I_0(t) \exp\left[-k_{PAR}(t) z_0\right] \, \mathrm{d}t}, \tag{3}$$

where the subscripts T and NT represent 'tidal' and 'non-tidal' parameters respectively, and angular brackets denote daily totals. Since times are measured relative to midday and L is the daylength, the limits of integration are from $-L/2$ (dawn) to $L/2$ (dusk). $F > 1$ indicates tidal amplification of seabed light, $F < 1$ indicates tidal reduction, and $F = 1$ indicates that the tide makes no discernible difference.

Eq. 3 can be solved numerically regardless of how I_0 and k_{PAR} are varied over the day. However, Bowers and Brubaker (2010) found that an approximate analytical solution can be obtained by making a number of simplifying assumptions. Firstly, k_{PAR} is treated as a constant over the day; to this end, a daily mean value, $\bar{k}_{PAR}$, suffices. Secondly, sea surface irradiance is approximated using a Gaussian curve, $I_0(t) = I_M \exp\left[-(t/q)^2\right]$, where I_M is the maximum (i.e., midday) surface irradiance, t is time (again measured relative to midday), and q is a parameter that controls the width of the Gaussian curve ($q \approx L/3$ offers a reasonable fit to observations of I_0 (Bowers and Brubaker, 2004)). Finally, tidally-varying water depth, z_T, is (re-)approximated as a parabola about low water by expanding the cosine term into its equivalent power series and retaining the first two terms only.

That is, $z_T = z_0 - b(1 - \omega^2(t - t_{lw})^2/2)$.

Substituting the above approximations into Eq. 3 ensures that both the integral in the numerator and that in the denominator have solvable forms, leading to the following analytical solution:

$$F = \sqrt{\frac{1}{x+1}} \exp\left[\bar{k}_{PAR} b\right](\exp[-\phi_1] + \exp[-\phi_2]), \tag{4}$$

where $x = 0.5\bar{k}_{PAR} b\omega^2 q^2$, and $\phi = (x/(x+1))(t_{lw}/q)^2$. Subscripts 1 and 2 on ϕ refer to its calculation using the time of either the first or second low water occurring in a day, respectively.

We have not reproduced here all intermediate steps in the derivation of this analytical solution. For these, the interested reader is referred to Bowers and Brubaker (2010).

Tidal photosynthesis amplification

A daily tidal photosynthesis amplification factor, Ψ, may be defined such that it is analogous to the daily tidal irradiance amplification factor, F.

$$\Psi = \frac{< P_{BT} >}{< P_{BNT} >} \tag{5}$$

$$= \frac{\int_{-L/2}^{L/2} P_{BT}(t)\ \mathrm{d}t}{\int_{-L/2}^{L/2} P_{BNT}(t)\ \mathrm{d}t}, \tag{6}$$

where P is the rate of (benthic algal) photosynthesis, subscripts denote either a 'tidal' or a 'non-tidal' parameter, angular brackets denote daily

totals of the enclosed parameters, and L is daylength. $\Psi > 1$ indicates tidal amplification of daily total seabed photosynthesis, $\Psi < 1$ indicates a tidal reduction, and $\Psi = 1$ indicates that the tide produces no discernible difference.

Photosynthesis-irradiance (P-I) curve equations

Data analysis and modelling aspects of this work are repeated using two different P-I curve parameterisations (Fig. 2): (1) the Peeters and Eilers (1978) Model, and (2) the Lederman and Tett (1981) Model.

The Peeters and Eilers (1978) P-I Model is appropriate at the thallus scale. It is mechanistic (rather than empirically derived) and includes the effect of photoinhibition. It has been used successfully to fit observed P-I curves for a common subtidal kelp species (*Saccharina latissima*) near our study site in Brittany (Gévaert et al., 2003). *Saccharina latissima* is found in the Bay of Brest (Hily et al., 1992) and is an excellent subject for the purpose of inferring / modelling photosynthesis in the subtidal zone.

Middelboe et al. (2006) found that, unlike for isolated thalli, the photosynthetic production of established macroalgal communities in shallow water tends not to become fully light-saturated or photoinhibited at the highest incident irradiances. The authors attributed this to a number of reasons associated with the species richness / composition of the community, and with canopy structure and density. We therefore repeat our analyses using the Lederman and Tett (1981) 'Rectangular Hyperbola'

163 P-I Model (i.e., no true saturation, no photoinhibition), which Middelboe
164 et al. (2006) used successfully to fit the P-I responses of shallow-water
165 macroalgal communities off Denmark.

166 Both equations are given below, and we use the subscripts t and c to
167 denote 'thallus-scale' and 'community-scale' parameters, respectively. Note
168 that throughout the present work we have effectively normalised rates of
169 thallus and community photosynthesis by their respective maxima. Thus,
170 the maximum ('normalised') photosynthesis achievable has a value of 1 in
171 both cases. This has the benefit that both thallus and community
172 photosynthesis can be plotted on the same axis or using the same scale for
173 straightforward comparison. We have expressed this 'normalised'
174 photosynthesis in arbitrary units, which are dimensionless. Values input
175 into the equations are given in Table 1. The Peeters and Eilers (1978)
176 equation is as follows:

$$P_t = \frac{I}{aI^2 + bI + c}, \tag{7}$$

177 where the coefficients a, b, and c dictate the precise shape of the curve.
178 These are, in turn, functions of key photosynthesis parameters, as follows:

$$a = \frac{1}{\alpha_t I_{m,t}^2},$$

$$b = \frac{1}{P_{m,t}} - \frac{2}{\alpha_t I_{m,t}},$$

and

$$c = \frac{1}{\alpha_t},$$

where $\alpha_t = P_{m,t}/I_{k,t}$ (i.e., the initial slope of the P-I curve, or light use efficiency), $P_{m,t}$ is the maximum possible rate of photosynthesis (n.b., in this study, P_t is the 'normalised' thallus photosynthesis discussed above, expressed in dimensionless arbitrary units, and thus we assign to $P_{m,t}$ a value of 1), $I_{k,t}$ is the saturation onset irradiance (i.e., the irradiance threshold beyond which photosynthesis begins to become light-saturated, or, more formally, the irradiance at which the initial slope of the P-I curve (extrapolated) intersects the maximum rate of photosynthesis, $P_{m,t}$), and $I_{m,t}$ is the optimum irradiance (i.e., the irradiance at which $P_{m,t}$ is achieved).

The Lederman and Tett (1981) equation is as follows:

$$P_c = \frac{\alpha_c P_{m,c} I}{P_{m,c} + \alpha_c I}, \tag{8}$$

where $\alpha_c = P_{m,c}/I_{k,c}$ (i.e., the initial slope of the P-I curve, or community light use efficiency), $P_{m,c}$ is the maximum photosynthesis achievable (n.b., P_c is the 'normalised' community photosynthesis discussed above, expressed in dimensionless arbitrary units, and thus we assign to $P_{m,c}$ a value of 1), and $I_{k,c}$ is the saturation onset irradiance for the community.

Materials and methods

Study site

The Bay of Brest (Fig. 3) is located at the westernmost extremity of the Brittany Peninsula in Northwest France, and has an area of approximately 180 km^2. It is connected to the Iroise Sea and the Atlantic Ocean beyond via a narrow, shallow channel (about 1.8 km wide, 4 km long, and, at its deepest, 50 m deep), known locally as 'Le Goulet'. The bay itself is shallower, with wide shoals and a mean depth of 10 m (Monbet and Bassoullet, 1989; Thouzeau et al., 2000).

The hydrodynamics of the Bay of Brest are dominated by tidal forcing. The average tidal range is 4.2 m, and ranges of up to 7.5 m are reached at large spring tides (Monbet and Bassoullet, 1989). Consequently, large exchanges of water occur through Le Goulet, and tidal currents there reach speeds of up to 2 m s^{-1} (Salomon and Breton, 1991). Freshwater input to the Bay of Brest (through the Élorn and Aulne Rivers) is small compared to the tidal exchanges with the Iroise Sea (Monbet and Bassoullet, 1989), and the bay is typically well-mixed (Delmas and Tréguer, 1983).

The phase of the solar semi-diurnal (or S_2) tidal constituent at the Bay of Brest is approximately 180° (expressed as a phase lag behind the corresponding constituent of the equilibrium tide at Greenwich) (Pingree and Griffiths, 1981). Consequently, the low waters of spring tides (LWST) always occur at about midday and midnight; at neaps, high waters occur at these times. Daylength at the site varies from approximately 8 h in winter

to 16 h in summer (calculated for the latitude of the study site using equations from Kirk (1994)). The Bay of Brest is less turbid than the Menai Strait (G. Chapalain, pers. comm.; Roberts et al., 2014). It can, however, still be considered 'coastal' in optical water type.

Observational campaigns

Fieldwork campaigns were undertaken in summer (July 2011) and winter (December 2011), and were approximately 2 and 3 weeks in length, respectively. During each campaign, two moorings were deployed simultaneously (as illustrated in Fig. 4) in the southern part of the Bay of Brest, near the town of Lanvéoc (see Fig. 3).

Tidally-modulated seabed irradiance, I_{BT}, was measured using an irradiance sensor in a bed frame (Fig. 4). This we will refer to as the 'tidal' mooring or condition. The sensor was fixed at 1.5 m above the seabed, and the frame was deployed in sufficiently deep water that it remained submerged at all stages of the tide. Its position was 48° 17.55′N 4° 26.96′W (see Fig. 3). A pressure sensor was fixed to the frame to allow the (tidally-varying) water depth, z_T, above the irradiance sensor to be monitored.

Irradiance beneath a fixed depth of water, I_{BNT}, was measured by suspending an identical irradiance sensor beneath a surface buoy (Fig. 4). The buoy and instrument were free to move vertically up and down with the sea surface, but the sensor remained submerged beneath a relatively

constant depth of water, z_{NT}. We will refer to this as the 'non-tidal' mooring or condition. Its position was 48° 17.79′N 4° 26.92′W (see Fig. 3). A pressure sensor was fitted to this mooring also, to check that variability in z_{NT} remained acceptably low. Several novel features were incorporated into the design of the 'non-tidal' mooring. These features helped to reduce instrument line swing/lean, to prevent excessive slack in the tether, and to permit the mooring to align freely with changing current directions. They are described fully in Roberts (2015). The combined effect was to maintain a relatively constant instrument depth and to prevent mooring self-entanglement.

Sea surface irradiance, I_0, was monitored using a third sensor positioned on the roof of the Centre d'Études Techniques Maritimes et Fluviales (CETMEF) at the Brest-Iroise Technopôle (48° 21.52′N 4° 34.01′W, Fig. 3). Prior to each fieldwork campaign, all sensors (i.e., irradiance and pressure sensors) were set to log measurements synchronously every 2 minutes.

We required that the contrived 'non-tidal' condition be comparable with the 'tidal' condition in terms of both mean water depth and clarity. The instrument on the 'non-tidal' mooring was positioned at a depth equal to the mean depth experienced by the 'tidal' instrument. This was determined in advance of deployment using tide tables, and verified after recovery using the pressure (depth) records. Both moorings were positioned as close together as was practically possible, so that they might experience similar conditions of water clarity. The 'non-tidal' mooring, however, was necessarily deployed in deeper water (i.e., further offshore) so that its

instrument was not grounded at low water.

A Lambert-Beer Law-based correction was applied to the I_{BNT} data to account for the fact that daily mean attenuation coefficients, $\bar{k}_{PAR}$, at the site of the 'non-tidal' mooring were consistently lower than at the site of the 'tidal' bed frame (in shallower, more turbid water). Time series of instantaneous k_{PAR} were calculated for both the 'tidal' and 'non-tidal' scenarios by using observations of sea surface irradiance, seabed irradiance, and water depth to solve Eq. 1 for k_{PAR}. Daily means, $\bar{k}_{PAR}$, were determined for both scenarios and the differences between corresponding daily means, $\Delta\bar{k}_{PAR}$ ($= \bar{k}_{PAR,tidal} - \bar{k}_{PAR,non-tidal}$), were used to correct (reduce) the appropriate instantaneous I_{BNT} values, according to $I_{BNT,corrected}(t) = I_{BNT,original}(t) \exp\left[-\Delta\bar{k}_{PAR} z_{NT}(t)\right]$. This correction effectively equates the daily mean attenuation coefficients of the two scenarios, whilst preserving the natural variability of the records.

The irradiance sensors were of type MDS-MkV/L (JFE Advantech, Kobe, Japan), which measure, and log internally, quantum scalar irradiance in the PAR waveband. Quantum scalar irradiance is the integral of the radiance distribution at a point, over all directions about that point (Kirk, 1994). Each instrument had been calibrated by the manufacturer against an LI-189 (LI-COR Biotechnology, Lincoln, Nebraska, USA) reference sensor, using a halogen light source. The manufacturers claim an accuracy of ± 4 % (full scale). Instrument resolution is 1 μmol quanta m^{-2} s^{-1}. The irradiance sensors used for this study were intercalibrated over a typical daily irradiance range at the School of Ocean Sciences (Bangor University,

Wales).

Additional corrections were applied to the irradiance data: (1) the typical dark current reading was deducted from all measurements before further analysis (after Topliss et al., 1980); (2) measurements from the two submerged sensors were multiplied by an 'immersion coefficient' to account for the so-called 'immersion effect' (Kirk, 1994); and (3) linear intercalibration equations (with coefficients that were averages of those determined pre- and post-fieldwork) were applied to account for slight differences in instrument sensitivities. Furthermore, a green-brown biofilm began to develop on the irradiance collectors after 2 weeks of summertime (July) deployment. The affected records were curtailed (post-recovery) at a length of 13 days to negate this concern.

Pressure sensors used were of the type DST Centi TD (Star Oddi Ltd., Reykjavík, Iceland). These are also internally-logging, and measure pressure with a resolution of 0.1 kPa (i.e., they can resolve approximately 1 cm changes of depth) and an accuracy of ± 1 kPa (i.e., approximately ± 10 cm water depth accuracy). The sensors were intercalibrated over a depth range of 0 - 8 m.

Atmospheric pressures were obtained from METAR (Meteorological Terminal Aviation Routine) reports generated hourly by the meteorological station at Lanvéoc-Poulmic Airbase ($48^\circ\,16.93'$N $4^\circ\,26.50'$W). A time series with 2 minute intervals was produced by interpolation. Atmospheric pressure was deducted from each measured pressure to isolate the component resulting from the overlying head of water alone. These values

were converted to water depths by dividing by the product of water density and acceleration due to gravity. Water density was calculated according to the International Equation of State of Sea Water (IES-80) using measured pressures and temperatures (recorded by the DST Centi sensors as a secondary parameter), and an estimate of mean salinity at the site (34 psu is appropriate (Delmas, 1981)). Acceleration due to gravity was calculated to be 9.81 m s^{-2} at the latitude of the Bay of Brest, using the International Gravity Formula (IGF).

Numerical model

Numerical model input values (Table 1) were selected to represent the Bay of Brest, and an individual thallus of *Saccharina latissima* or an established macroalgal community growing there. A 1 h time step was used.

Sea surface irradiance, $I_0(t)$, was modelled over a year using the following equation (from Gates (1980)):

$$I_0(N,t) = I_{Atmos}(N)\sin(\alpha(N,t))\exp\left[-k_{Atmos}m_{Air}(N,t)\right], \qquad (9)$$

where I_{Atmos} is the solar irradiance incident upon a surface perpendicular to the Sun's rays just outside Earth's atmosphere (in this study we are interested only in the PAR component - see Table 1 footnote), α is the solar altitude, k_{Atmos} is an atmospheric attenuation coefficient (which we have assumed to be a constant and have treated as a tunable parameter, and which represents a spectral average), m_{Air} is the air mass ratio, N is the day number (N=0 on January 1^{st}), and t is time, measured in hours from

the start of the day.

I_{Atmos} varies over the year, as a result of the elliptical orbit of the Earth about the Sun, according to $I_{Atmos}(N) = I_{SC}(1 + 0.0344\cos(360°N/365))$ (Kreith and Kreider, 1978; Duffie and Beckman, 2013), where I_{SC} is the solar constant - the irradiance (in this case, the PAR component only) received by a surface perpendicular to the Sun's rays just outside Earth's atmosphere at the mean Earth-Sun distance (see Table 1).

Solar altitude, α, is the angular elevation of the Sun above the horizon, and was calculated using the equation first developed by Milankovitch (1930): $\sin(\alpha(N,t)) = \sin(\gamma)\sin(\delta(N)) - \cos(\gamma)\cos(\delta(N))\cos(360°t/24)$, where γ is the latitude (in degrees), and δ is the solar declination (in degrees), the angle through which a given hemisphere is tilted towards (or away from) the Sun. δ was, in turn, calculated using $\delta(N) = 23.45\sin(360°(N + 284)/365)$ (Cooper, 1969; Brock, 1981).

The air mass ratio, m_{Air}, is the ratio of the optical path length through the atmosphere in the direction of the Sun, at an angle of α, to the path length in the vertical direction (i.e., with the Sun directly overhead at the zenith position) (Gates, 1980). We employed the commonly used approximation (Gates, 1980; Kumar et al., 1997) of $m_{Air} = 1/\sin(\alpha)$.

Eq. 9 is essentially a restatement of the Lambert-Beer Law, with the irradiance arriving at the outer atmosphere being attenuated exponentially as it propagates towards the sea surface. The additional $\sin(\alpha)$ factor, not found in the Lambert-Beer Law, represents an adjustment to I_{Atmos} (which is defined for a surface perpendicular to the Sun's rays) to account for the

fact that extraterrestrial solar radiation may be obliquely incident upon the local zenith (see Gates (1980) for diagrams illustrating geometric considerations). The form of Eq. 9 results in a continuous sine wave output, from which only the non-negative values are of relevance to our northern hemisphere site. Negative values were set to zero by the model script to represent night-time irradiances, which may be considered negligible for our purposes.

Seabed irradiance time series (i.e., $I_{BT}(t)$ and $I_{BNT}(t)$) were computed as $I_0(t)$ attenuated exponentially by the product of water depth, $z(t)$, and diffuse attenuation coefficient of PAR, $k_{PAR}(t)$, again in accordance with the Lambert-Beer Law (Eq. 1).

To obtain 'tidal' seabed irradiance, $I_{BT}(t)$, a tidally-varying water depth was used. This was modelled as the sum of a lunar and a solar semi-diurnal tide (i.e., the M_2 and S_2 tidal constituents respectively), to produce a semi-diurnal and a springs-neaps cycle. The phase of the S_2 constituent was set to 180° to ensure the low waters of spring tides always occurred at midday and midnight, as is approximately the case at the Bay of Brest.

$k_{PAR}(t)$ was modelled as daily mean values (i.e., $\bar{k}_{PAR}$) varying from day to day with daily mean tidal range, $\bar{R}$, as follows

$$\bar{k}_{PAR}(N) = (\frac{1}{2} + \frac{1}{2}\cos\frac{2\pi N}{365})m\bar{R}(N) + c \tag{10}$$

where N is again day of the year, and m and c are constants. We return to the form of this equation below. $\bar{R}$(N) was modelled as a cosine function with a springs-neaps periodicity; the mean, amplitude, period and phase

was set precisely by the M_2 and S_2 parameters in Table 1. k_{PAR} was not varied on shorter timescales (e.g., during the day with the semi-diurnal tide).

Irradiance and depth observations (see 'Observational campaigns') together permitted the calculation of $\bar{k}_{PAR}$ values for each day of the two campaigns (not shown). In winter, a scattered but statistically significant (at the 95% confidence level) positive linear relationship between $\bar{k}_{PAR}$ and $\bar{R}$ was observed. In summer, however, the relationship was not statistically significant (at the 95% confidence level). Hence, we modelled the variation of $\bar{k}_{PAR}$ with $\bar{R}$ over a year using Eq. 10, which is that of a straight line with an intercept, c, representing a baseline value of $\bar{k}_{PAR}$, and a gradient that varies incrementally throughout the year, from m in mid-winter (i.e., $\bar{k}_{PAR} = m\bar{R} + c$) to 0 in mid-summer (i.e., $\bar{k}_{PAR} = c$ for all $\bar{R}$). The gradient variation between m and 0 is achieved by means of the bracketed 'gradient modifier', a cosinusoidal function of annual periodicity, varying between 1 in mid-winter and 0 in mid-summer. m and c values used in the model are based on the winter observations, and are given in Table 1.

To obtain 'non-tidal' seabed irradiance, $I_{BNT}(t)$, the mean water depth was applied at all times, t. The choice of $k_{PAR}(t)$ parameterisation was determined by the desired output. For daily amplification factors, daily mean values of k_{PAR} ($\bar{k}_{PAR}$) were used here also (i.e., $k_{PAR}(t)$ was modelled, as for the 'tidal' case, using Eq. 10). This is because the Bowers and Brubaker (2010) definition of daily tidal irradiance amplification requires that $\bar{k}_{PAR}$ values used in both 'tidal' and 'non-tidal' cases be equal

399 on any given day. For the output of springs-neaps amplification factors and
400 for annual calculations, the 'non-tidal' k_{PAR} was held constant (i.e., set to
401 the mean of the $\bar{k}_{PAR}$ values generated by Eq. 10) over each springs-neaps
402 cycle or over the year, respectively.

403 Modelled $I_{BT}(t)$ and $I_{BNT}(t)$ were initially input into the Peeters and
404 Eilers (1978) *P-I* Equation (7) to provide $P_{BT}(t)$ and $P_{BNT}(t)$ appropriate
405 at the thallus scale. Similarly, modelled $I_{BT}(t)$ and $I_{BNT}(t)$ were input into
406 the Lederman and Tett (1981) *P-I* Equation (8) to provide $P_{BT}(t)$ and
407 $P_{BNT}(t)$ appropriate at the community scale. Daily, springs-neaps, and
408 annual totals of these outputs, for use in calculating amplification factors,
409 were determined by numerical integration (i.e., trapezium rule) with
410 respect to time. Daily tidal amplification factors for irradiance, F, and
411 photosynthesis, Ψ, were calculated according to Equations 2 and 5,
412 respectively. Springs-neaps and annual irradiance and photosynthesis
413 amplification factors (i.e., F_{SN}, Ψ_{SN}, F_{ANN}, and Ψ_{ANN}) were determined
414 similarly:

$$F_{SN} = \frac{< I_{BT} >_{SN}}{< I_{BNT} >_{SN}}, \tag{11}$$

$$\Psi_{SN} = \frac{< P_{BT} >_{SN}}{< P_{BNT} >_{SN}}, \tag{12}$$

$$F_{ANN} = \frac{< I_{BT} >_{ANN}}{< I_{BNT} >_{ANN}}, \tag{13}$$

415 and

$$\Psi_{ANN} = \frac{< P_{BT} >_{ANN}}{< P_{BNT} >_{ANN}}, \tag{14}$$

where angular brackets with the subscripts SN or ANN denote springs-neaps or annual totals of the enclosed parameters, respectively.

Results

Tidal irradiance amplification determined from observations

Time series observations and daily tidal irradiance amplification factors, F, from the summer and winter campaigns are presented in Figures 5 and 6, respectively. Throughout the summer campaign, observed F values were close to unity (Fig. 5(d)), ranging from 1.0 to 1.3. No clear springs-neaps cycle in F was apparent. In the winter dataset, however, F values exhibited a strong springs-neaps cycle (Fig. 6(d)), being much larger at spring tides (up to 31.5) than at neap tides (as low as 0.4).

Agreement between observed and theoretically predicted tidal irradiance amplification (using Eq. 4) is demonstrated graphically in Figure 7. The analytical solution appears to perform well for the Bay of Brest. Model II regression (i.e., the major axis method (Ricker, 1973)) performed on the combined summer and winter data gave a slope of 1.311±0.050 and an intercept of -0.63±0.15. t-tests (two-tailed) were conducted to compare these values with the slope and intercept that would be expected in the case of perfect agreement between observations and predictions (i.e., 1 and 0, respectively). There were statistically significant differences (at the 95%

confidence level) between both the slopes ($t = 6.25$, $df = 32$, $p < 0.001$) and the intercepts ($t = -4.10$, $df = 32$, $p < 0.001$). This departure from 'perfect agreement' reflects the relatively modest shortcomings of an analytical solution in which several assumptions were employed (see Bowers and Brubaker, 2010). The solution shows a tendency to overpredict at larger amplifications.

Tidal photosynthesis amplification determined from inferred photosynthesis

Fig. 8 illustrates (using a subset of our irradiance time series observations, and rates of photosynthesis inferred from these observations), some conditions under which photosynthesis amplification factors, Ψ, and irradiance amplification factors, F, may converge or differ.

On 12th July (left hand panels, Fig. 8), overcast conditions ensure irradiances in both 'tidal' and 'non-tidal' scenarios remain below the saturation onset irradiance of an individual thallus for much of the day, and below that of an established community for the entire day. Consequently, photosynthesis responds approximately linearly to irradiance throughout the day (in both 'tidal' and 'non-tidal' cases, and for both thallus and community). Computed thallus and community Ψ values are therefore both similar to the prevailing F value (F=1.16, cf. Ψ(thallus)=1.08 and Ψ(community)=1.11).

On 13th July (right hand panels, Fig. 8) the sky was relatively

cloud-free, and the day correspondingly brighter. Tidal irradiance amplification is clearly apparent by comparing the areas beneath the 'tidal' and 'non-tidal' irradiance curves. Thallus photosynthesis is light-saturated (and even photoinhibited) in both 'tidal' and 'non-tidal' scenarios for much of the day (note how P_B approximately flatlines in both scenarios between about 8am and 5pm). There is no appreciable photosynthesis amplification at the thallus scale, and thus Ψ(thallus) departs from F (F=1.23, cf. Ψ(thallus)=1.02). In contrast, the P-I curve parameterisation adopted here to describe community photosynthesis does not truly saturate, and inferred community photosynthesis continues to respond at these elevated irradiances. In the 'tidal' community photosynthesis curve a local maximum can be seen at low water (∼9am), and the curve is somewhat depressed around high water (∼3pm). Consequently, some tidal photosynthesis amplification occurs at the community scale, such that F and Ψ(community) are closer in value (F=1.23, cf. Ψ(community)=1.11).

Exploring the F-Ψ relationship with a numerical model

In Fig. 8, differences in sea surface irradiation from one day to the next, owing to differences in cloud cover, provided a convenient way to illustrate how F and Ψ may converge or differ. However, cloud cover is often ephemeral and changes with little temporal regularity. Here, we explore the more regular, predictable aspects of the F-Ψ relationship using the simple numerical model described earlier (see Materials and methods).

Output in which daily changes are resolved is shown in Fig. 9 for a mean water depth of 4.1 m (i.e., 1 m below the level of LWST) in the Bay of Brest. This corresponds approximately to the mean depth of our observations. Modelled F behaviour (Fig. 9(b)) compares favourably with the winter and summer observations. A springs-neaps pattern in F is present throughout the year; peaks are at spring tides (when low water is at midday) and troughs are at neaps (when high water is at midday). The amplitude of the cycle is large in winter (modelled F varies from 0.66 to 11.72), when short daylengths exaggerate the difference between springs and neaps. It is considerably reduced in summer (modelled F varies from 0.97 to 1.64), when the days are longer.

Modelled Ψ behaviour at the thallus scale (Fig. 9(c)) corresponds with that of F in winter, but a 'switch' in the sense of the springs-neaps pattern occurs near the equinoxes. Longer summer daylengths permit the morning and evening low waters of neap tides to occur within daylight hours. This boosts the tidally-modulated photosynthesis (i.e., P_{BT}) at neaps. Consequently, they become more beneficial, in photosynthesis amplification terms, than spring tides, where a single, large pulse of seabed light around the midday low water saturates or inhibits P_{BT} (at this depth and time of year).

At the community scale, the springs-neaps cycle in Ψ does not 'switch sense' to peak at neap tides during the summer months. Instead, Ψ 'flatlines' at a value of approximately 1 throughout the summer (Fig. 9(d)). The mechanism responsible is the same as that invoked above to explain

499 the 'switch'. The effects are less dramatic for the case of macroalgal
500 communities (i.e., a reduction, to nothing, of the amplitude of the
501 springs-neaps cycle in Ψ, rather than a switch of sense) because
502 communities do not become truly light-saturated or photoinhibited
503 (Middelboe et al., 2006). Convergence of springs and neaps Ψ values upon
504 a value of 1 during the summer months suggests that the tide has neither
505 an amplifying or a reducing effect on community photosynthesis at these
506 longer daylengths, and at this depth, in the Bay of Brest.

507 Fig. 10 shows F_{SN}, Ψ_{SN} (at the thallus scale), and Ψ_{SN} (at the
508 community scale) modelled over a year at 1 m below the level of LWST in
509 the Bay of Brest. At the thallus scale, F_{SN} and Ψ_{SN} do not correspond very
510 closely; values of $\Psi_{SN}(thallus)$ are suppressed by the increased prevalence
511 of light-saturation and photoinhibition in this scenario. In the summer,
512 tidal (i.e., springs-neaps) reduction of thallus photosynthesis occurs (i.e.,
513 $\Psi_{SN}(thallus) < 1$), despite tidal amplification of irradiance (i.e., $F_{SN} > 1$).

514 At the community scale, the magnitudes and temporal behaviour of Ψ_{SN}
515 more closely approach those of F_{SN}. No appreciable tidal reduction of
516 photosynthesis is sustained through summer. This can again be explained
517 by the absence of true light-saturation in the community-scale P-I curve
518 parameterisation. Even the largest maxima in tidally-modulated seabed
519 irradiance, occurring at (the midday) LWST during summer, do not present
520 a macroalgal community with such a 'photosynthetic disadvantage' (i.e.,
521 prolonged saturation or photoinhibition) as they do an individual/isolated
522 kelp thallus in shallow water.

The annual tidal irradiance amplification factor, F_{ANN}, output by the model for a depth of 1 m below the level of LWST in the Bay of Brest was 2.33. The annual photosynthesis amplification factors at the thallus and community scales, $\Psi_{ANN}(thallus)$ and $\Psi_{ANN}(community)$, for the same depth were 1.06 and 1.42, respectively.

Discussion

Observations in the Bay of Brest

The key physical parameters controlling the magnitude of the tidal irradiance amplification effect (on a given day) were identified by Bowers and Brubaker (2010) to be the diffuse attenuation coefficient, k_{PAR}, the tidal range, R (or amplitude, b), the times of low water relative to noon, t_{lw}, and the daylength, L. In a qualitative sense, our observations in the Bay of Brest support this. In winter, the amplification is large at springs when R is large, k_{PAR} is elevated generally, and low water occurs at midday. Reduction occurs at neaps when R and k_{PAR} are smaller, and high water occurs at midday. This springs-neaps pattern appears to be modulated also by the seasonal cycle in daylength: it is pronounced in winter, when short days exaggerate the consequences of having either low water or high water at midday (i.e., springs and neaps respectively); it is not present in summer, when longer days permit the irradiance 'gains' of the midday LWST, or 'losses' of the midday HWNT (high water neap tide), to be offset somewhat

by the morning and evening high waters, or low waters, respectively.

Agreement between existing theory and observation has, in this paper, been demonstrated quantitatively also. Comparison of observed daily tidal irradiance amplification factors, F_{Obs}, with those predicted for the conditions on each day, F_{Pred}, using the analytical solution of Bowers and Brubaker (2010) (a function of the 4 key parameters outlined above) shows reasonable agreement. Much of the key physics underlying tidal amplification is included in the analytical solution and, based on the fact that it has performed well for two sites with contrasting tidal regimes (i.e., the Menai Strait in the earlier work (Bowers and Brubaker, 2010) and the Bay of Brest in the current work), it can be expected to perform at least reasonably well for many more, perhaps most, coastal sites with a semi-diurnal tide.

As a caveat to the above, we note that a tidal cycle in k_{PAR} is present at the Bay of Brest (not shown in this paper). As for the Menai Strait (Roberts et al., 2014) and the Tamar Estuary (Pilgrim and Millward, 1989, and references therein), the cycle is out of phase with the tidal curve, reaching a maximum at low water and a minimum at high water. The Bowers and Brubaker (2010) solution assumes constant k_{PAR} over the day, and employs the daily mean value in predicting F. This was necessary in order to make the analytical solution possible. The consequence is that the solution tends to overpredict F on days where the k_{PAR} tidal cycle is particularly distinct (e.g., on 27th December $F_{Obs} = 31.5$, whereas $F_{Pred} = 43.4$ (see Fig. 6 and 7)).

Whilst we have insufficient data to say anything conclusive about the nature of the mechanism driving the tidal cycle in k_{PAR}, we speculate, as did Pilgrim and Millward (1989), that it involves the local resuspension of sediment by increased turbulence at low water. It could, therefore, be common to many shallow, coastal sites. At other sites, k_{PAR} behaviour may exhibit clear cycles with quarter-diurnal or semi-diurnal frequency, owing to tidal resuspension or tidal advection of suspended particulate matter (SPM) respectively (e.g., Weeks et al. (1993) and Williams et al. (1998)). In any case, an analytical solution of comparable simplicity to that of Bowers and Brubaker (2010), which incorporates such regular patterns in k_{PAR}, is difficult to achieve. Use of the Bowers and Brubaker (2010) solution to make predictions for sites with appreciable and inherent k_{PAR} cycles will incur some error, and the interested investigator is advised to model the tidal irradiance amplification effect (including the k_{PAR} variability) numerically in these cases.

An irradiance sensor in a simple bed frame provided the 'tidal' irradiance data in the present work, whereas a novel mooring was designed and employed to allow irradiance in the hypothetically equivalent 'non-tidal' condition to be measured directly, rather than inferred from surface irradiance records. This new mooring performed encouragingly well: it provided high quality, continuous time series data for each campaign; it did not become entangled, despite tidal currents and, occasionally, strong wind forcing; and, most importantly, it successfully held the irradiance sensor at a relatively constant water depth over time.

590 Two limitations are associated with the use of this mooring. Firstly,
591 whilst the irradiance data is rendered independent of tidal variations in
592 water depth by the mooring, it is not independent of the tidal variations in
593 k_{PAR} discussed above. Thus, it is not comprehensively 'non-tidal' data but,
594 given that the tidal range in the Bay of Brest is typically much greater than
595 the range in k_{PAR}, it is sufficiently so for our purposes. Secondly, the
596 'non-tidal' mooring was deployed further offshore than the 'tidal' bed frame.
597 This allowed the requirement of equal mean depths to be satisfied, whilst
598 preventing the 'non-tidal' sensor from becoming grounded at low water. As
599 a consequence, the daily mean k_{PAR} (i.e., $\bar{k}_{PAR}$), as experienced by the
600 'non-tidal' sensor, was consistently lower than at the shallower 'tidal' bed
601 frame site. This is not desirable ($\bar{k}_{PAR}$ should be approximately equal in
602 both conditions) and necessitated the application of a Lambert-Beer-based
603 correction (see 'Materials and methods') to the 'non-tidal' data.

604 A workaround exists for the second limitation: deploy the bed frame
605 further offshore also, elevating its sensor considerably to maintain the same
606 mean depth. This is logistically much less practical, however, both in terms
607 of the deployability of the adapted (larger) frame and of the increased
608 danger to shipping in these relatively busy, shallow waters.

Numerical modelling predictions

609 The following key predictions emerged out of the modelling study, and
610 apply to the shallow sub-tidal (i.e., 1 m below the level of LWST) in the

Bay of Brest:

- Annual total seabed irradiance is amplified by the tide (by a factor of 2.33 relative to a 'non-tidal' but otherwise equivalent scenario). Annual total photosynthesis at the seabed is hardly amplified at all by the tidal irradiance amplification (i.e., by a factor of just 1.06) at the isolated, individual thallus scale, but is more substantially amplified at the established macroalgal community scale (i.e., by a factor of 1.42).

- When considered at springs-neaps resolution, tidal modulation of seabed irradiance is of greatest significance, in terms of its influence on the photosynthesis of benthic algae, during winter (when it results in amplification of photosynthesis at both community and thallus scales). It is of less significance during summer, when it has a negligible effect at the community scale and results in a modest, sustained reduction in photosynthesis at the thallus scale.

- At finer temporal resolution, a springs-neaps cycle is present in the daily tidal irradiance amplification factor. Peaks are at spring tides, troughs are at neap tides, and the amplitude of the cycle is large in winter and considerably smaller in summer (in agreement with our observations). The daily tidal photosynthesis amplification factor exhibits a similar pattern during winter at both the thallus and community scales. During summer, however, this pattern 'switches

sense' (such that the peaks are at neap tides) at the thallus scale, and 'flatlines' (at a value of approximately 1) at the community scale.

As noted previously, the springs-neaps cycle in daily tidal irradiance amplification factor peaks at spring tides because a low water occurs at about midday during springs at the Bay of Brest. Conversely, troughs are at neap tides because a high water occurs at midday at these times. The amplitude of the cycle is larger in winter because shorter daylengths exaggerate the difference between these two situations. The irradiance-amplifying potential of spring tides in winter also accounts for amplification predicted over longer timescales (i.e., the amplification occurring during winter at the springs-neaps timescale, and the overall annual amplification).

Whether tidal amplification of seabed light produces a similar amplification of seabed photosynthesis depends on how light levels compare with the saturation onset irradiance of a given species or community. Below this threshold, rates of photosynthesis respond approximately linearly to the time course of instantaneous irradiance, and photosynthesis amplification corresponds with the prevailing irradiance amplification. Should irradiances exceed this threshold (as occurs more frequently in summer), the relationship between irradiance amplification and photosynthesis amplification becomes more complex, and (as we have shown) their respective factors may differ. The response of the isolated, individual thallus and that of the established macroalgal community will

differ in this respect because their photosynthesis-irradiance characteristics are different (Gévaert et al., 2003; Middelboe et al., 2006): a kelp thallus may become light-saturated and even photoinhibited, but an established macroalgal community is unlikely to become truly light-saturated. Generally, the consequence is that, at the thallus scale, photosynthesis amplification factors readily depart from their corresponding irradiance amplification factors (including the case whereby photosynthesis is reduced despite irradiance being amplified by the tide), whilst at the community scale, there is likely to be a more consistently positive correlation between tidal irradiance amplification and photosynthesis amplification.

The numerical model was constructed using widely accepted parameterisations of key physical and biological processes. For example, surface irradiance was modelled using well-known equations found in Gates (1980), Kirk (1994), and others, the attenuation of irradiance with water depth was modelled using the Lambert-Beer Law, tidally-varying water depth was modelled as the sum of two sinusoidal tidal constituents (M_2 and S_2), and P-I curves were modelled with the Peeters and Eilers (1978) Equation (appropriate at the thallus scale) and the Lederman and Tett (1981) Equation (appropriate at the community scale). The main limitations of the work are associated with the use of photosynthesis parameters, controlling the precise shape of the P-I curves, that are unchanging over time.

In fact, the shape of a P-I curve exhibits a dependence on water temperature and substrate (i.e., CO_2) availability, both of which are liable

to change, to varying degrees, over the timescales considered here (Dring, 1992; Hurd et al., 2014). Furthermore, a P-I curve can be temporally dynamic owing to mechanisms endogenous to the alga, particularly those which permit it to maximise its performance in any situation (Delebecq et al., 2013). Notably, algae are known to acclimate to changes in the intensity and spectral quality of the ambient light, on timescales ranging from minutes to months, by adjustments to their photosynthetic apparatus (Dring, 1992; Kirk, 1994; Falkowski and Raven, 1997; Hurd et al., 2014). Short-term adjustments (e.g., minutes to days) include changes to the Photosystem II absorption cross-section, changes to the position and orientation of chromatophores, and photoprotective mechanisms, such as non-photochemical quenching (i.e., the harmless dissipation of excess light energy as heat) (Nultsch and Pfau, 1979; Müller et al., 2001; Duarte et al., 2013). Longer-term adjustments (e.g., days to months) include changes to pigment content and composition (Kirk, 1994).

Duarte et al. (2013) noted that P-I curve parameters should be considered as variables rather than constants. As discussed, these variables are functions of many environmental parameters (e.g., temperature, CO_2 concentration, ambient light intensity and quality) and have, as yet, not been parameterised satisfactorily. We chose to employ a 'static', or fixed, P-I curve taken from the literature when modelling photosynthesis over time from modelled irradiance (as did Zimmerman et al. (1994)). Whilst this is likely to be a reasonable first order approximation (see Middelboe et al., 2006), the accuracy of model estimates / predictions will undoubtedly

be improved if studies like those of Gévaert et al. (2003) and Duarte et al. (2013) can be built upon to provide generalisable parameterisations of a *P-I* curve's 'dynamic' nature.

The are a number of broad implications of the modelling study that can be extended to sites other than they Bay of Brest. Demonstrated for the first time in this work, the effect of the tide in amplifying or reducing time-integrated seabed light is likely to induce a similar effect on time-integrated benthic photosynthesis. These effects are likely to be more strongly coupled at the macroalgal community scale (which is arguably more ecologically relevant than that of the isolated thallus). To extend comments made by Bowers and Brubaker (2010), just as error will be introduced to modelled estimates of seabed light if tidal effects are neglected, for example by employing a mean water depth and clarity over time, the same is likely to be true of modelled estimates of seabed photosynthesis. At many sites, neglecting the tidal effects will lead to underestimates of time-integrated irradiance and photosynthesis in the subtidal zone.

We have shown that the time course of benthic photosynthesis and time-integrated benthic photosynthesis in the shallow subtidal appear to be controlled, at least in part, by the tidal characteristics of the site in question, through their modulation of seabed irradiance (i.e., the times of low water, t_{lw}, and their advance through the springs-neaps cycle, and the tidal range, R, and its variability). Observed differences in these aspects of benthic photosynthesis from site to site may be attributable to differences

in t_{lw}, R, k_{PAR} and L behaviour between the sites, rather than (or in addition to) abiotic and biotic factors identified in the literature to date.

We speculate that there may be a second important spatial (i.e., depth) component to the effect of tidal modulation of seabed light on benthic photosynthesis and ecology. Since subtidal benthic algae are readily light-limited, and different species possess different light requirements/tolerances, it is natural to hypothesise that such an effect might influence the depth distribution of these species differentially, in turn influencing characteristics of the prevailing benthic community such as depth gradients in species composition, vertical zonation patterns, and overall areal extent and algal cover. A modelling approach such as the one adopted here cannot be employed to investigate this until the effects of photoacclimation on photosynthesis parameters (in the depth dimension) have been adequately quantified and parameterised for key species. This is a problem of considerable importance to the field of modelling shallow-water benthic productivity, and is our primary recommendation as a direction for future research.

In terms of the practical relevance of this work, habitat managers and policy makers should be aware that projects which alter the tidal characteristics of a particular coastline, such as the construction of barrages or lagoons for tidal energy extraction, and the changes to tides that are predicted to occur with sea-level variability (e.g., Neill et al., 2010) are likely to affect the time course of photosynthesis in, and the overall productivity of, benthic plants and algae, through the tide's influence on

752 the available seabed light.

References

753 Ackleson, S.G., 2003. Light in shallow waters : A brief research review.
754 Limnology and Oceanography 48, 323–328.

755 Bowers, D.G., Brubaker, J.M., 2004. Underwater sunlight maxima in the
756 Menai Strait. Journal of Optics A: Pure and Applied Optics 6, 684–689.

757 Bowers, D.G., Brubaker, J.M., 2010. Tidal amplification of seabed light.
758 Journal of Geophysical Research 115, C09008.

759 Bowers, D.G., Tett, P., Walne, A.W., 1997. A note on seabed irradiance in
760 shallow tidal seas. Journal of the Marine Biological Association of the
761 United Kingdom 77, 921–928.

762 Brock, T.D., 1981. Calculating solar radiation for ecological studies.
763 Ecological Modelling 14, 1–19.

764 Cooper, P.I., 1969. The absorption of solar radiation in solar stills. Solar
765 Energy 12, 333–346.

766 Delebecq, G., Davoult, D., Menu, D., Janquin, M.A., Dauvin, J.C.,
767 Gévaert, F., 2013. Influence of local environmental conditions on the
768 seasonal acclimation process and the daily integrated production rates of
769 Laminaria digitata (Phaeophyta) in the English Channel. Marine Biology
770 160, 503–517.

771 Delmas, R., 1981. Étude de l'évolution saisonnière des sels nutritifs dans
772 la rade de Brest en fonction des apports fluviaux et des échanges avec
773 l'Iroise. Ph.d. thesis. Université de Bretagne Occidentale, Brest.

774 Delmas, R., Tréguer, P., 1983. Évolution saisonnière des nutriments dans
775 un écosystème eutrophe d'Europe Occidentale (la rade de Brest).
776 lnteractions marines et terrestres. Oceanologica Acta 6, 345–355.

777 Dring, M.J., 1992. The biology of marine plants. Cambridge University
778 Press, Cambridge.

779 Duarte, P., Ramos, M., Calado, G., Jesus, B., 2013. Laminaria hyperborea
780 photosynthesis-irradiance relationship measured by oxygen production and
781 pulse-amplitude-modulated chlorophyll fluorometry. Aquatic Biology 19,
782 29–44.

783 Duffie, J.A., Beckman, W.A., 2013. Solar engineering of thermal
784 processes. John Wiley and Sons, Hoboken. Fourth edition.

785 Falkowski, P.G., Raven, J.A., 1997. Aquatic photosynthesis. Blackwell,
786 Oxford.

787 Gates, D.M., 1980. Biophysical Ecology. Springer-Verlag, New York.

788 Gévaert, F., Créach, A., Davoult, D., Holl, A.C., Seuront, L., Lemoine, Y.,
789 2002. Photo-inhibition and seasonal photosynthetic performance of the
790 seaweed Laminaria saccharina during a simulated tidal cycle: chlorophyll

fluorescence measurements and pigment analysis. Plant, Cell and Environment 25, 859–872.

Gévaert, F., Créach, A., Davoult, D., Migné, A., Levavasseur, G., Arzel, P., Holl, A.C., Lemoine, Y., 2003. Laminaria saccharina photosynthesis measured in situ: photoinhibition and xanthophyll cycle during a tidal cycle. Marine Ecology Progress Series 247, 43–50.

Heck, K.L., Hays, G., Orth, R.J., 2003. Critical evaluation of the nursery role hypothesis for seagrass meadows. Marine Ecology Progress Series 253, 123–136.

Hily, C., Potin, P., Floc'h, J.Y., 1992. Structure of subtidal algal assemblages on soft-bottom sediments: fauna/flora interactions and role of disburbances in the Bay of Brest, France. Marine Ecology Progress Series 85, 115–130.

Hurd, C.L., Harrison, P.J., Bischof, K., Lobban, C.S., 2014. Seaweed ecology and physiology. Cambridge University Press, Cambridge.

Kirk, J.T.O., 1994. Light and photosynthesis in aquatic ecosystems. Cambridge University Press, Cambridge. Second edition.

Kreith, F., Kreider, J.F., 1978. Principles of solar engineering. McGraw-Hill, New York.

Kumar, L., Skidmore, A.K., Knowles, E., 1997. Modelling topographic variation in solar radiation in a GIS environment. International Journal of Geographical Information Science 11, 475–497.

Lederman, T.C., Tett, P., 1981. Problems in modelling the photosynthesis-light relationship for phytoplankton. Botanica Marina 43, 305–314.

Mann, K.H., 1972. Ecological energetics of the sea-weed zone in a marine bay on the Atlantic coast of Canada. II. Productivity of the seaweeds. Marine Biology 14, 199–209.

Middelboe, A.L., Sand-Jensen, K., Binzer, T., 2006. Highly predictable photosynthetic production in natural macroalgal communities from incoming and absorbed light. Oecologia 150, 464–476.

Milankovitch, M., 1930. Mathematische klimalehre und astronomische theorie der klimaschwankungen. Handbuch der Klimatologie, Band I, Teil A. Gebruder Borntraeger, Berlin.

Monbet, Y., Bassoullet, P., 1989. Bilan des connaissances océanographiques en rade de Brest. Rapport CEA/IPSN, code DERO/EL 89-23, IFREMER-DEL-BP 70-29280. Technical Report. IFREMER. Plouzané.

Müller, P., Li, X.P., Niyogi, K.K., 2001. Non-Photochemical Quenching. A Response to Excess Light Energy. Plant Physiology 125, 1558–1566.

831 Naylor, E., 2010. Chronobiology of marine organisms. Cambridge
832 University Press, Cambridge.

833 Neill, S.P., Scourse, J.D., Uehara, K., 2010. Evolution of bed shear stress
834 distribution over the northwest European shelf seas during the last 12,000
835 years. Ocean Dynamics 60, 1139–1156.

836 Nultsch, W., Pfau, J., 1979. Occurrence and biological role of light-induced
837 chromatophore displacements in seaweeds. Marine Biology 51, 77–82.

838 Peeters, J.C.H., Eilers, P., 1978. The relationship between light intensity
839 and photosynthesis - a simple mathematical model. Hydrobiological
840 Bulletin 12, 134–136.

841 Pilgrim, D.A., Millward, G.E., 1989. Variation in the diffuse optical depth
842 of the bed of a tidal estuary, in: McManus, J., Elliott, M. (Eds.),
843 Developments in Estuarine and Coastal Study Techniques. Olsen and
844 Olsen, Fredensborg, pp. 101–107.

845 Pingree, R.D., Griffiths, D.K., 1981. S2 tidal simulations on the
846 north-west European shelf. Journal of the Marine Biological Association of
847 the United Kingdom 61, 609–616.

848 Ricker, W.E., 1973. Linear regressions in fishery research. Journal of the
849 Fisheries Research Board of Canada 30, 409–434.

850 Roberts, E.M., 2015. Tidal modulation of seabed light and its implications
851 for benthic algae. Ph.D. thesis. Bangor University.

852 Roberts, E.M., Bowers, D.G., Davies, A.J., 2014. Springs-neaps cycles in
853 daily total seabed light: Daylength-induced changes. Journal of Marine
854 Systems 132, 116–129.

855 Salomon, J.C., Breton, M., 1991. Numerical study of the dispersive
856 capacity of the Bay of Brest, France, towards dissolved substances., in:
857 Lee, J.H.W., Cheung, Y.K. (Eds.), Environmental Hydraulics, Balkema,
858 Rotterdam. pp. 459–464.

859 Steneck, R.S., Graham, M.H., Bourque, B.J., Corbett, D., Erlandson,
860 J.M., Estes, J.A., Tegner, M.J., 2002. Kelp forest ecosystems: biodiversity,
861 stability, resilience and future. Environmental Conservation 29, 436–459.

862 Thouzeau, G., Chauvaud, L., Grall, J., Guérin, L., 2000. Rôle des
863 interactions biotiques sur le devenir du pré-recrutement et la croissance de
864 Pecten maximus (L.) en rade de Brest. Comptes Rendus de l'Académie
865 des Sciences - Series III - Sciences de la Vie 323, 815–825.

866 Topliss, B.J., Hunter, J.R., Simpson, J.H., 1980. Simultaneous
867 measurements of transparency and irradiance in the coastal waters of
868 North Wales. Marine Environmental Research 4, 65–79.

869 Weeks, A.R., Simpson, J.H., Bowers, D.G., 1993. The relationship
870 between concentrations of suspended particulate material and tidal
871 processes in the Irish Sea. Continental Shelf Research 13, 1325–1334.

872 Williams, J.J., Humphery, J.D., Hardcastle, P.J., Wilson, D.J., 1998. Field
873 observations of hydrodynamic conditions and suspended particulate matter
874 in the southern North Sea. Continental Shelf Research 18, 1215–1233.

875 Zimmerman, R.C., Cabello-Pasini, A., Alberte, R.S., 1994. Modeling daily
876 production of aquatic macrophytes from irradiance measurements: a
877 comparative analysis. Marine Ecology Progress Series 114, 185–196.

Acknowledgements

878 This work was supported by the Natural Environment Research Council
879 [Grant Number NE/I527853/1]. Fieldwork in Brest was made possible
880 thanks to the following people: Georges Chapalain, Alexis Beudin and
881 Antoine Douchin, of CETMEF (now Cerema); IUEM (Institut Universitaire
882 Européen de la Mer) scientists and technicians working on the CHIVAS
883 (chimie des valves de la Coquille Saint-Jacques Européennes) project; and
884 the captain and crew of R.V. Albert Lucas. Mervyn and Susan Roberts,
885 and Yvon and Christiane Lainé kindly provided logistical support and
886 accommodation. Malen Jukes and Geraint Roberts are thanked for
887 commenting on the manuscript. Two anonymous reviewers are thanked for
888 their suggestions, which led to considerable improvements to this work.

Figure legends

1 Schematic demonstrating how the exponential attenuation of irradiance, I, with depth, z, can lead to tidal amplification (after Bowers and Brubaker (2010)). The disproportionately large 'gain' in tidally-modulated seabed irradiance, I_{BT}, at low tide (compared to that at mid tide) is not matched by the similarly defined 'loss' at high tide. The magnitude of the amplification will depend upon the diffuse attenuation coefficient, k_{PAR} (which controls the rate of exponential attenuation with depth), and the tidal range, R. Sea surface irradiance, I_0, varies throughout the day (not illustrated), meaning that the timing of low waters, t_{lw}, and the daylength, L, are also important.

2 Photosynthesis-irradiance (P-I) curves generated using the two equations employed in this study. The Peeters and Eilers (1978) Model (Eq. 7) is appropriate for thallus-scale photosynthesis, and input values used to produce the curve are representative of *Saccharina latissima* (values from Gévaert et al., 2003). The Lederman and Tett (1981) Model (Eq. 8) is appropriate for macroalgal community-scale photosynthesis, and input values used were from Middelboe et al. (2006). See Table 1 for input values.

3 The Bay of Brest study site at the western extremity of the Brittany Peninsula (inset). Deployed instrumentation is indicated with black squares and a bold typeface (see text for details).

4 Schematic of the moorings deployed to observe tidal irradiance amplification.

5 Summer campaign time series data. Panel (a) shows sea surface irradiance, I_0; (b) shows tidally-modulated seabed irradiance, I_{BT}, and water depth, z_T, from the bed frame; and (c) shows 'non-tidal' sub-surface irradiance, I_{BNT}, and water depth, z_{NT}, from the surface-moored frame. Panel (d) displays daily tidal irradiance amplification factors, F, determined in accordance with Eq. 2 (daily irradiance totals estimated by numerical integration using the trapezium rule). Note the $\log_{10}$ scale used on the vertical axis. Grey-shaded areas represent night-time.

926 6 Winter campaign time series data. Panel (a) shows sea sur-
927 face irradiance, I_0; (b) shows tidally-modulated seabed irra-
928 diance, I_{BT}, and water depth, z_T, from the bed frame; and
929 (c) shows 'non-tidal' sub-surface irradiance, I_{BNT}, and wa-
930 ter depth, z_{NT}, from the surface-moored frame. Panel (d)
931 displays daily tidal irradiance amplification factors, F, deter-
932 mined in accordance with Eq. 2 (daily irradiance totals es-
933 timated by numerical integration using the trapezium rule).
934 Note the $\log_{10}$ scale used on the vertical axis. Grey-shaded
935 areas represent night-time.

936 7 Predicted daily tidal irradiance amplification factors, F_{Pred},
937 generated using the Bowers and Brubaker (2010) analytical
938 solution (Eq. 4), plotted against the observed values, F_{Obs}.
939 Logarithmically-scaled axes provide improved clarity at small
940 F values, where all of the summer points and about half of
941 the winter points are clustered. The dashed line represents
942 the hypothetical case whereby theory and observation agree
943 perfectly.

8 Conditions under which photosynthesis amplification factors, Ψ, and irradiance amplification factors, F, may converge (left hand panels) or differ (right hand panels). See text for explanation. Irradiances are observed values (30 minute averages). Rates of photosynthesis are inferred using the relevant *P-I* equations (see Theory). Times of low and high waters are denoted by LW and HW respectively in the uppermost panels.

9 Numerical model output over a year at 1 m below the level of LWST. Panel (a) shows daily mean tidal range, $\bar{R}$, and its springs-neaps variation, for reference. (b) shows the daily tidal irradiance amplification factor, F. (c) and (d) show the analogously defined daily tidal photosynthesis amplification factor, Ψ, determined at the thallus and community scales, respectively. Peaks in F and Ψ are labelled S (springs) or N (neaps) to denote the sense of cycles at various times of year. The sense 'switching' behaviour of cycles in Ψ at the thallus scale, and the lack thereof at the community scale, is discussed in the text. Input values were representative of the Bay of Brest, and of a thallus of *Saccharina latissima* (in the case of (c)) or an established macroalgal community (in the case of (d)).

10 Springs-neaps irradiance amplification factors, F_{SN}, and springs-neaps photosynthesis amplification factors, Ψ_{SN}, output by the numerical model for a depth of 1 m below LWST in the Bay of Brest. Two Ψ_{SN} curves are shown, representing model runs with P-I parameterisations appropriate at the thallus scale and at the community scale. The dash-dotted line indicates the threshold above which amplification is said to have occurred and below which reduction has occurred.

Tables

Table 1: Input parameters and their values for the numerical model. Surface irradiance and tidal parameters were selected to be representative of the Bay of Brest. Photosynthesis parameters were selected to be representative of a thallus of *Saccharina latissima* or an established macroalgal community (see text).

Parameter	Symbol(s)	Value
Sea surface irradiance parameters		
Latitude of Bay of Brest	γ	48.3°
Solar constant (PAR component)*	I_{SC}	2400 μmol quanta m^{-2} s^{-1}
Atmospheric attenuation coeff.	k_{Atmos}	0.01
Tidal cycle parameters		
M_2 period	-	12.421 h
S_2 period	-	12 h
M_2 amplitude	-	2.1 m
S_2 amplitude	-	1.0 m
M_2 phase	-	0°
S_2 phase	-	180°
$\bar{k}_{PAR}$ **variation parameters (dependence on** $\bar{R}$**)**		
Max. (winter) gradient	m	0.1 m^{-2}
Intercept	c	0.4 m^{-1}
Photosynthesis parameters		
Max. rate of photosyn.	$P_{m,t}$, $P_{m,c}$	1 (arbitrary units)
Optimum irradiance**	$I_{m,t}$	300 μmol quanta m^{-2} s^{-1}
Saturation onset irrad.**	$I_{k,t}$	100 μmol quanta m^{-2} s^{-1}
Saturation onset irrad.***	$I_{k,c}$	291 μmol quanta m^{-2} s^{-1}

* A solar constant of 1373 W m^{-2} (total solar irradiance) is assumed, of which approximately 38% (521.74 W m^{-2}) is PAR (Kirk, 1994). This is multiplied by the approximate conversion factor 4.6 μmol quanta J^{-1}, which arises from assuming PAR has a mean wavelength of 550 nm, to provide the PAR component in the appropriate units for this study. ** Approximated from Gévaert et al. (2003), and applied to the thallus-scale *P-I* equation (Eq. 7). *** Value from Middelboe et al. (2006), and applied to the community-scale *P-I* equation (Eq. 8).

Figures

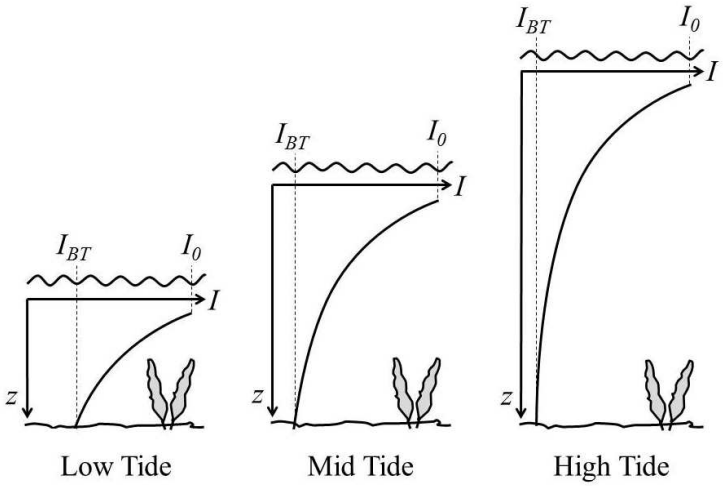

Figure 1: Schematic demonstrating how the exponential attenuation of irradiance, I, with depth, z, can lead to tidal amplification (after Bowers and Brubaker (2010)). The disproportionately large 'gain' in tidally-modulated seabed irradiance, I_{BT}, at low tide (compared to that at mid tide) is not matched by the similarly defined 'loss' at high tide. The magnitude of the amplification will depend upon the diffuse attenuation coefficient, k_{PAR} (which controls the rate of exponential attenuation with depth), and the tidal range, R. Sea surface irradiance, I_0, varies throughout the day (not illustrated), meaning that the timing of low waters, t_{lw}, and the daylength, L, are also important.

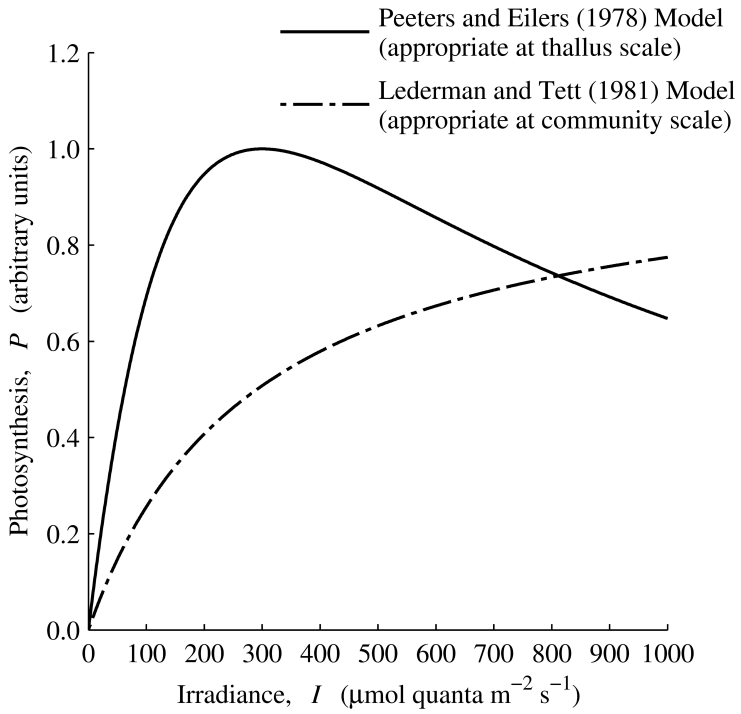

Figure 2: Photosynthesis-irradiance (P-I) curves generated using the two equations employed in this study. The Peeters and Eilers (1978) Model (Eq. 7) is appropriate for thallus-scale photosynthesis, and input values used to produce the curve are representative of *Saccharina latissima* (values from Gévaert et al., 2003). The Lederman and Tett (1981) Model (Eq. 8) is appropriate for macroalgal community-scale photosynthesis, and input values used were from Middelboe et al. (2006). See Table 1 for input values.

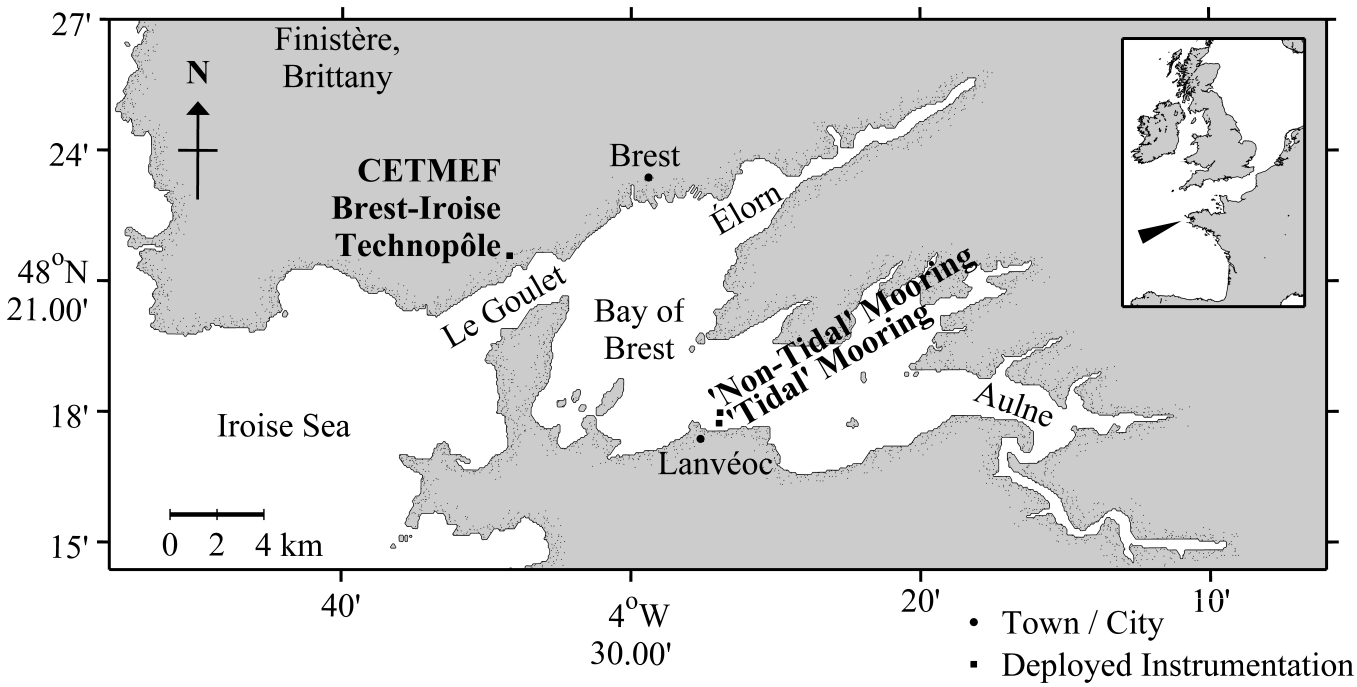

Figure 3: The Bay of Brest study site at the western extremity of the Brittany Peninsula (inset). Deployed instrumentation is indicated with black squares and a bold typeface (see text for details).

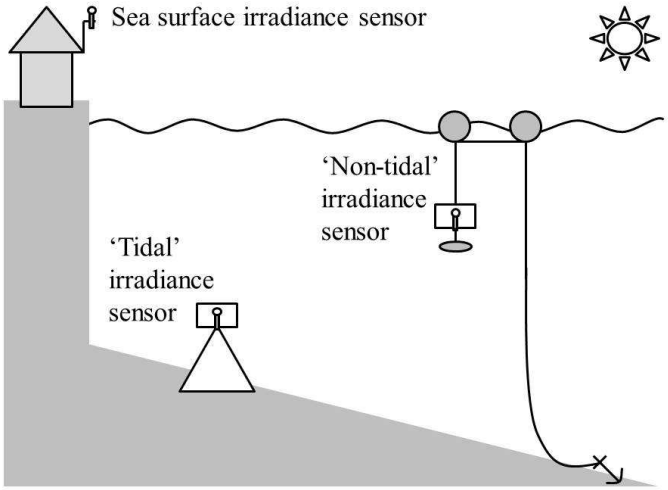

Figure 4: Schematic of the moorings deployed to observe tidal irradiance amplification.

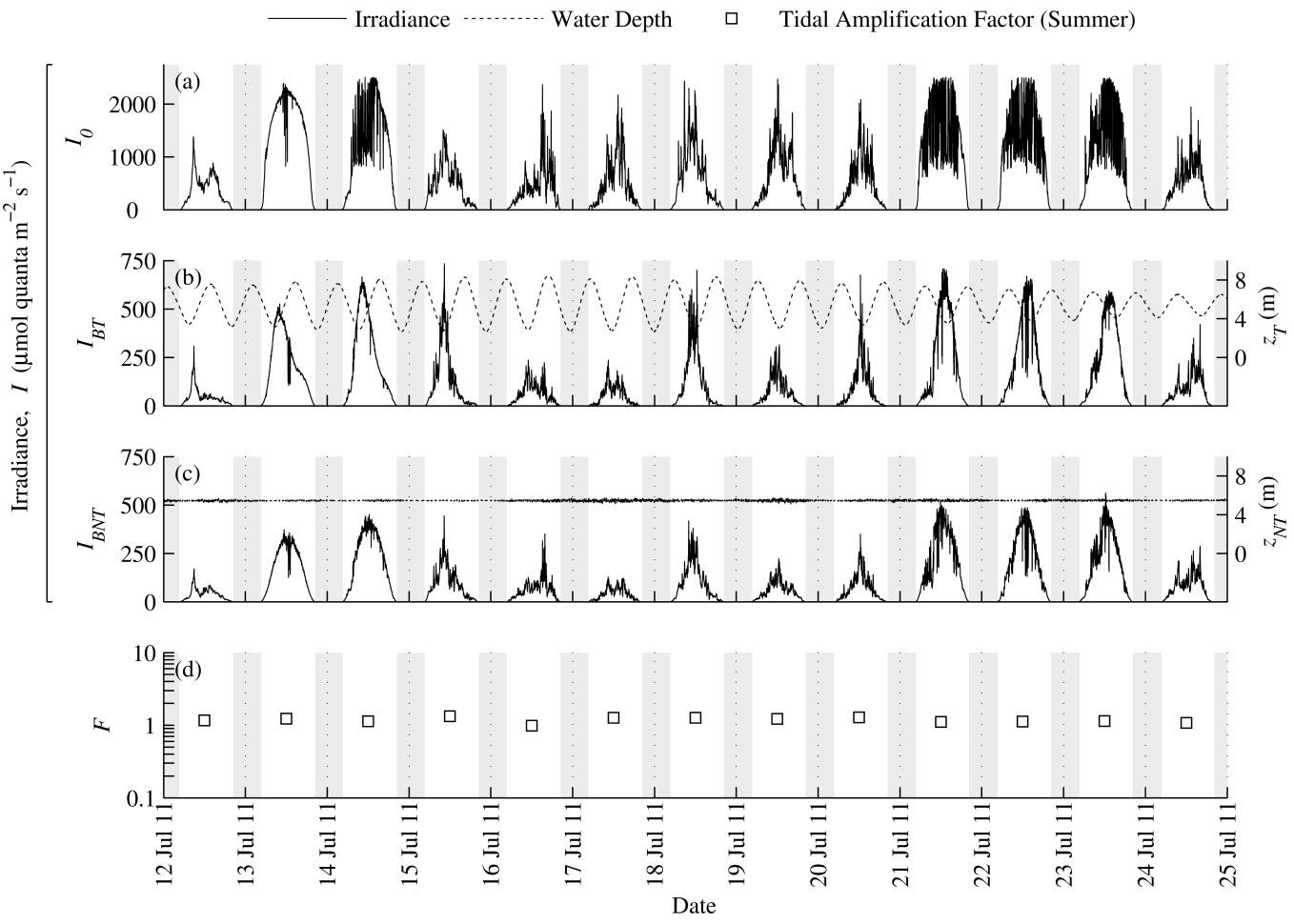

Figure 5: Summer campaign time series data. Panel (a) shows sea surface irradiance, I_0; (b) shows tidally-modulated seabed irradiance, I_{BT}, and water depth, z_T, from the bed frame; and (c) shows 'non-tidal' sub-surface irradiance, I_{BNT}, and water depth, z_{NT}, from the surface-moored frame. Panel (d) displays daily tidal irradiance amplification factors, F, determined in accordance with Eq. 2 (daily irradiance totals estimated by numerical integration using the trapezium rule). Note the $\log_{10}$ scale used on the vertical axis. Grey-shaded areas represent night-time.

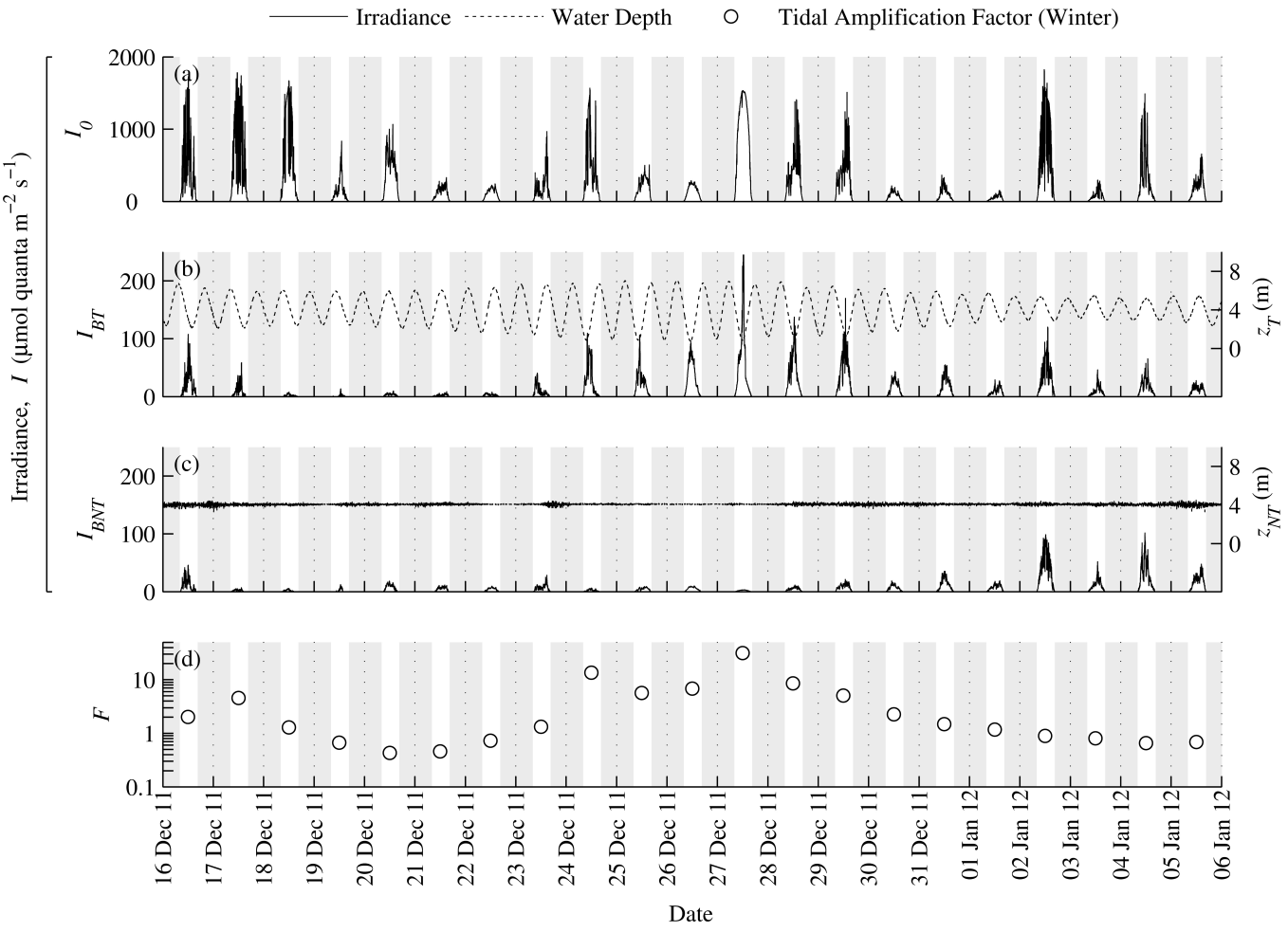

Figure 6: Winter campaign time series data. Panel (a) shows sea surface irradiance, I_0; (b) shows tidally-modulated seabed irradiance, I_{BT}, and water depth, z_T, from the bed frame; and (c) shows 'non-tidal' sub-surface irradiance, I_{BNT}, and water depth, z_{NT}, from the surface-moored frame. Panel (d) displays daily tidal irradiance amplification factors, F, determined in accordance with Eq. 2 (daily irradiance totals estimated by numerical integration using the trapezium rule). Note the $\log_{10}$ scale used on the vertical axis. Grey-shaded areas represent night-time.

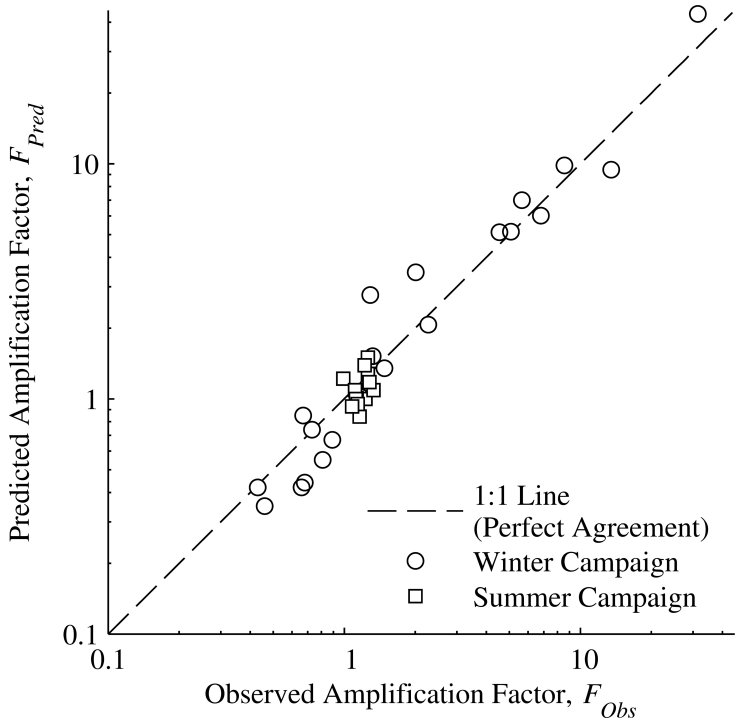

Figure 7: Predicted daily tidal irradiance amplification factors, F_{Pred}, generated using the Bowers and Brubaker (2010) analytical solution (Eq. 4), plotted against the observed values, F_{Obs}. Logarithmically-scaled axes provide improved clarity at small F values, where all of the summer points and about half of the winter points are clustered. The dashed line represents the hypothetical case whereby theory and observation agree perfectly.

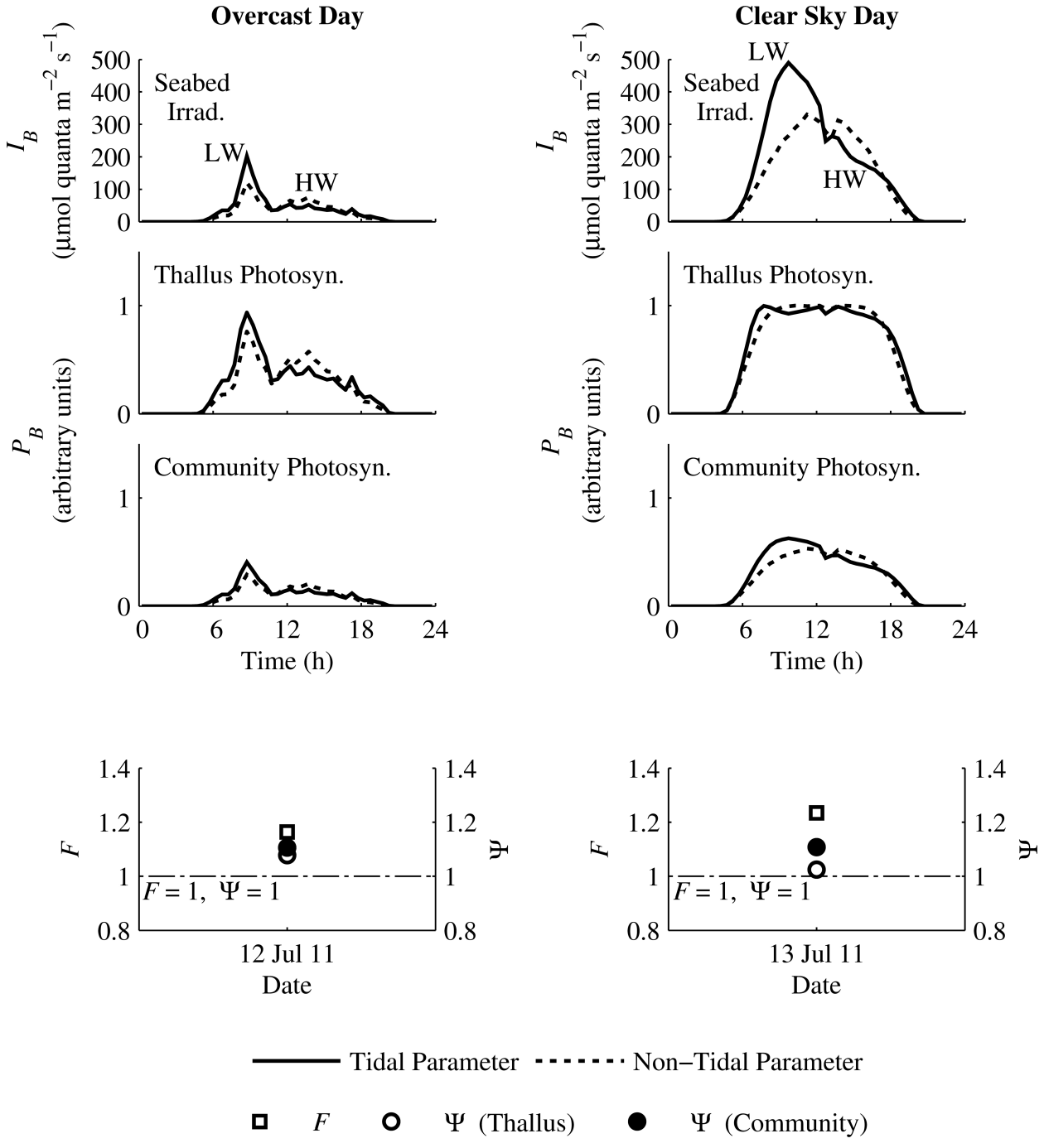

Figure 8: Conditions under which photosynthesis amplification factors, Ψ, and irradiance amplification factors, F, may converge (left hand panels) or differ (right hand panels). See text for explanation. Irradiances are observed values (30 minute averages). Rates of photosynthesis are inferred using the relevant P-I equations (see Theory). Times of low and high waters are denoted by LW and HW respectively in the uppermost panels.

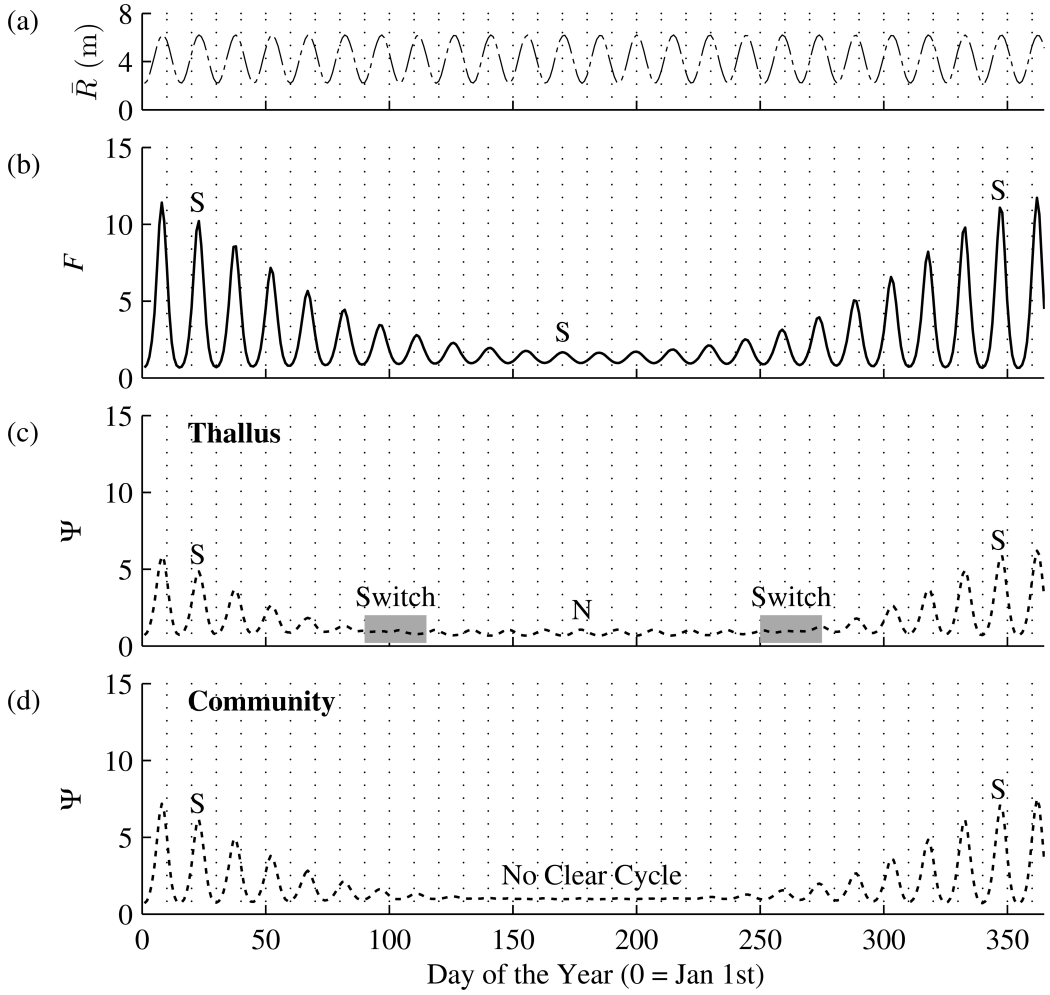

Figure 9: Numerical model output over a year at 1 m below the level of LWST. Panel (a) shows daily mean tidal range, $\bar{R}$, and its springs-neaps variation, for reference. (b) shows the daily tidal irradiance amplification factor, F. (c) and (d) show the analogously defined daily tidal photosynthesis amplification factor, Ψ, determined at the thallus and community scales, respectively. Peaks in F and Ψ are labelled S (springs) or N (neaps) to denote the sense of cycles at various times of year. The sense 'switching' behaviour of cycles in Ψ at the thallus scale, and the lack thereof at the community scale, is discussed in the text. Input values were representative of the Bay of Brest, and of a thallus of *Saccharina latissima* (in the case of (c)) or an established macroalgal community (in the case of (d)).

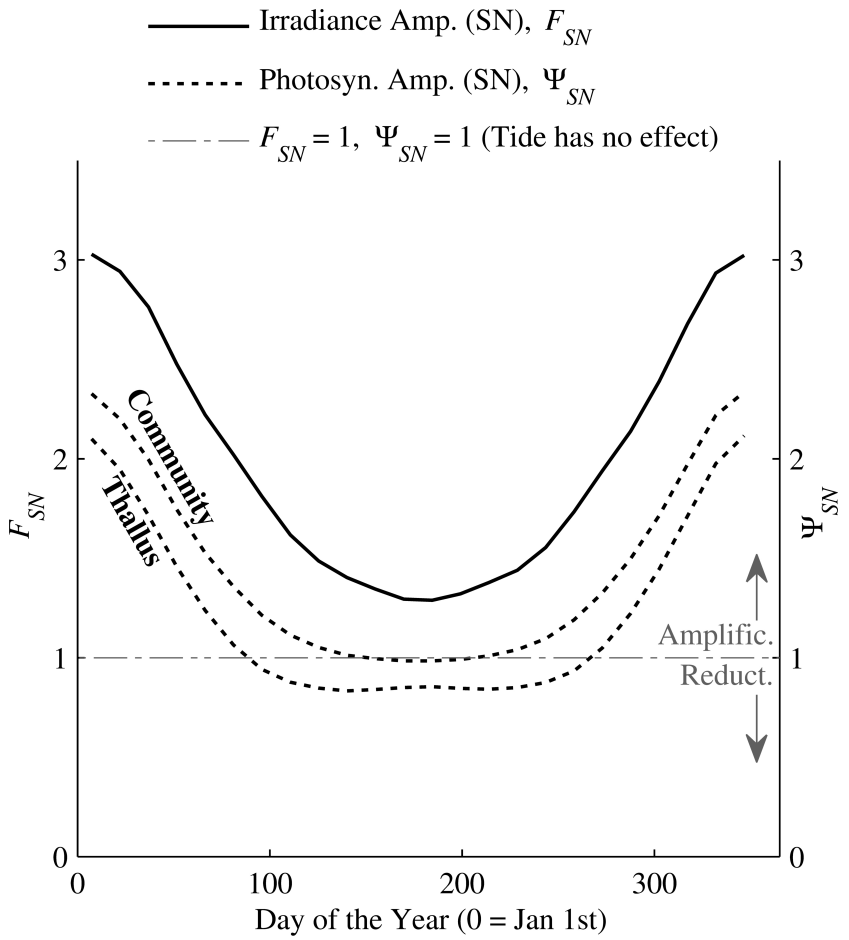

Figure 10: Springs-neaps irradiance amplification factors, F_{SN}, and springs-neaps photosynthesis amplification factors, Ψ_{SN}, output by the numerical model for a depth of 1 m below LWST in the Bay of Brest. Two Ψ_{SN} curves are shown, representing model runs with P-I parameterisations appropriate at the thallus scale and at the community scale. The dash-dotted line indicates the threshold above which amplification is said to have occurred and below which reduction has occurred.